A Proposed Classification of Intraretinal Microvascular Abnormalities in Diabetic Retinopathy Following Panretinal Photocoagulation

Akito Shimouchi,[1] Akihiro Ishibazawa,[1] Satoshi Ishiko,[1,2] Tsuneaki Omae,[1] Tomoko Ro-Mase,[1] Yasuo Yanagi,[1] and Akitoshi Yoshida[1]

[1]Department of Ophthalmology, Asahikawa Medical University, Asahikawa, Japan
[2]Medicine and Engineering Combined Research Institute, Asahikawa Medical University, Asahikawa, Japan

Correspondence: Akihiro Ishibazawa, Department of Ophthalmology, Asahikawa Medical University, Midorigaoka Higashi 2-1-1-1, Asahikawa 078-8510, Japan; bazawa14@asahikawa-med.ac.jp.

Received: May 6, 2019
Accepted: January 16, 2020
Published: March 19, 2020

Citation: Shimouchi A, Ishibazawa A, Ishiko S, et al. A proposed classification of intraretinal microvascular abnormalities in diabetic retinopathy following panretinal photocoagulation. *Invest Ophthalmol Vis Sci.* 2020;61(3):34. https://doi.org/10.1167/iovs.61.3.34

Purpose. To investigate the characteristics of intraretinal microvascular abnormalities (IRMAs) before and after panretinal photocoagulation (PRP) for diabetic retinopathy (DR) by using optical coherence tomography angiography (OCTA).

Methods. Forty-six eyes of 29 patients with DR were included (26 eyes with severe nonproliferative diabetic retinopathy [SNPDR] and 20 eyes with proliferative diabetic retinopathy [PDR]). En face OCTA images of IRMAs in a 6 × 6-mm area were acquired by using Cirrus 5000 with AngioPlex. The morphological changes in IRMAs were evaluated before and after PRP. The changes in the IRMAs were divided into five subtypes: unchanged; tuft regression; reperfusion; mixed (combined tuft regression/reperfusion); and worsening (new appearance of tuft).

Results. Unchanged IRMAs were identified in 15 SNPDR eyes and 2 PDR eyes; all neovascularization (NV) had regressed after PRP. Tufts were more frequently observed in the PDR eyes (15/20, 75%) than in the SNPDR eyes (8/26, 31%) ($P = 0.003$), and two tufts tended to exceed the inner limiting membrane, which showed progression to NV before PRP. The reperfusion phenomenon was observed in 7/26 SNPDR eyes and 4/20 PDR eyes, including the mixed type, and showed two vascular patterns: abnormal (dilated, tortuous, and twisted) and normal vessels. The worsening type was observed in 1/26 SNPDR eye and 2/20 PDR eyes.

Conclusions. OCTA enabled classification of IRMA into more detailed types. The unchanged and reperfusion types suggested that IRMAs had aspects of remodeling. However, IRMAs with tufts were observed in 75% of the PDR eyes, and the tufts had aspects of NV.

Keywords: optical coherence tomography, optical coherence tomography angiography, diabetic retinopathy, intraretinal microvascular abnormality

In 1981, the Diabetic Retinopathy Study used standardized photographs to define intraretinal microvascular abnormalities (IRMAs) as tortuous intraretinal vascular segments in fields, varying in caliber from barely visible to 31 mm per the Early Treatment Diabetic Retinopathy Study.[1–3] IRMAs are one of the hallmarks of end-stage nonproliferative diabetic retinopathy (DR),[4] with its severity being a risk factor of progression to proliferative diabetic retinopathy (PDR).[5] IRMAs are therefore regarded as an important clinical endpoint as defined in the international severity classification.[6] Despite such clinical consensus, subclassification of IRMAs remains controversial. The histopathological characteristics of IRMAs were described prior to clinical definitions by Ashton in 1953.[7] He described them as new dilated channels situated midway between arteries and veins that projected toward the arteries and communicated with the venous capillary circulation, and they were associated with obliteration of circulation on the arterial side. In fluorescein angiography (FA), IRMAs have little or no leakage and can generally be differentiated from neovascularization (NV).[8,9] IRMAs on FA appear to flow into a vein while originating from a vein.[10] The traditional view was that IRMAs represent vascular remodeling that corresponds to the enlargement of capillary nonperfusion. However, in 1984, Muraoka and Shimizu[11] proposed the concept of intraretinal neovascularizations (IRNVs) in which revascularization of nonperfused area (NPA) was observed in nonproliferative retinopathy with subsequent proliferative changes appearing later, suggesting that some IRMAs are forme fruste of retinal NV. A subsequent study supported that a substantial proportion of patients with diabetes have IRNVs when repeated angiography is performed.[12] Interestingly, Lee et al.[13] in their study reported that transition from IRMA to NV commenced with an initial outpouching of the inner limiting membrane (ILM) without the disruption of this layer. However, despite the firm evidence showing that some IRMAs (i.e., IRNVs) are precursor lesions of neovascularization elsewhere (NVE), subclassification of IRMAs by FA have limited clinical

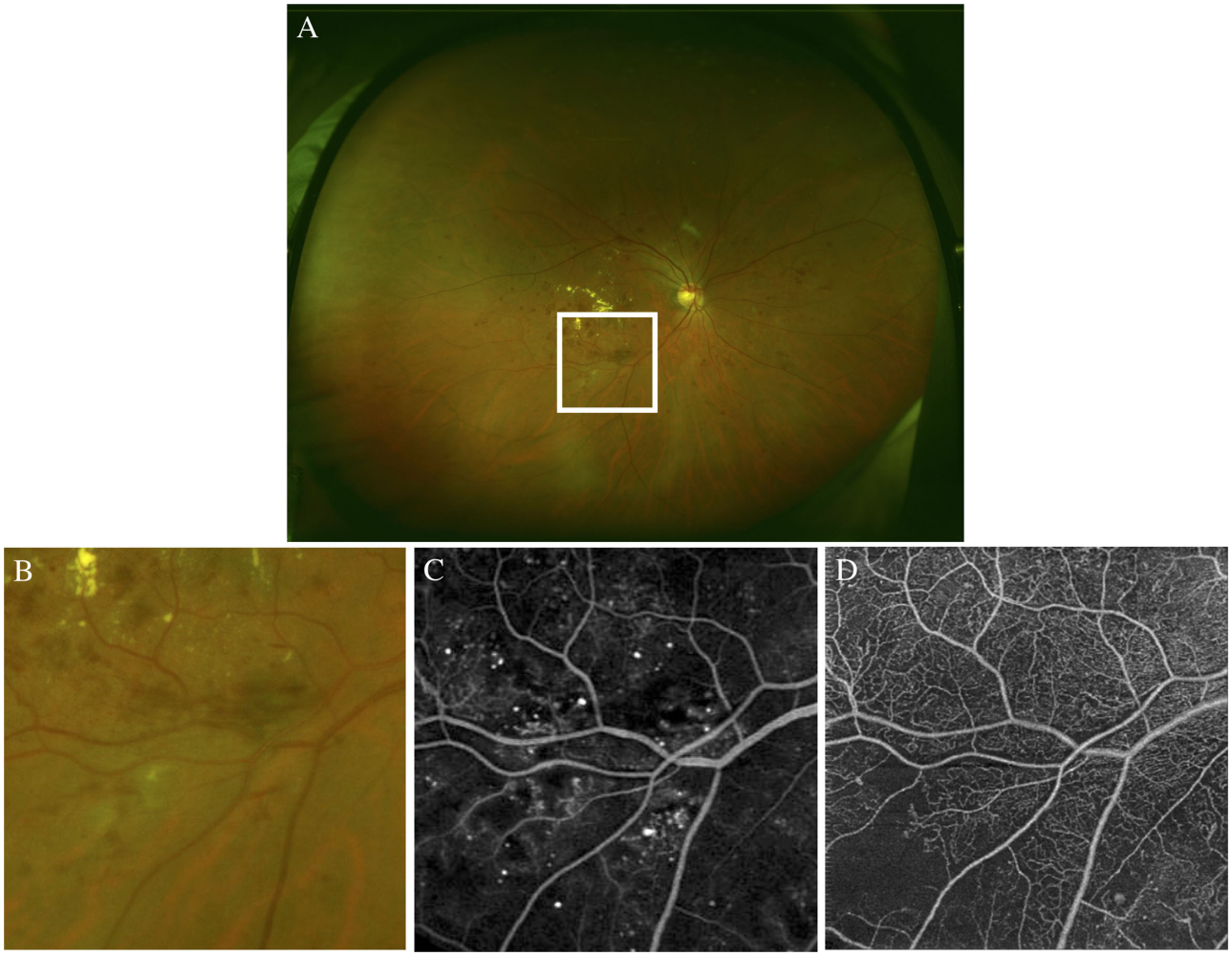

Figure 1. Comparison of how NV, IRMAs, and the NPA are captured for each fundus image examination. (**A**) Color fundus photograph of the whole retina with PDR. The *white square* outlines the area shown on the angiogram. (**B**) Magnified color fundus photograph image of the area surrounded by a *white square*. (**C**) Magnified FA image in the same area as that of the color fundus photograph image. (**D**) OCTA image of all layers in a 6 × 6-mm area. The scanning area of OCTA was guided by the fundus observation of tortuous abnormal vascular lesions and the FA leakage.

significance in disease monitoring, in part because FA is an invasive examination that is not preferred/practical in patients with diabetes, and spaciotemporal resolution of FA images is limited.

Recently developed noninvasive optical coherence tomography angiography (OCTA) is useful for observing vascular lesions in DR and can clearly visualize the NPA and adjacent IRMA and NV with high contrast.[14] OCTA was reported to detect 50% of IRMA cases that were missed on color fundus photography (CFP) images.[15] Our group has recently evaluated the characteristics of NV before and after panretinal photocoagulation (PRP) using OCTA and reported that robust vascular proliferation can be an active sign of NV.[16] In the current study, we extended our OCTA study and evaluated the morphological changes in IRMAs before and after PRP. We noted that there are dynamic changes in the morphology of IRMAs and aim in this report to highlight distinct progression and regression patterns of IRMAs based on OCTA.

Methods

Inclusion Criteria and Data Collection

Clinical and imaging data were collected retrospectively from patients of the Asahikawa Medical University from February 1, 2016 to December 31, 2017. This study adhered to the tenets of the Declaration of Helsinki. Approvals for data collection and analyses were obtained from the institutional review board of the Asahikawa Medical University. The inclusion criteria involved new or previous diagnosis of severe nonproliferative diabetic retinopathy (SNPDR), or treatment-naive PDR, or previously treated PDR that still had active NV after deficient retinal photocoagulation (PC). The included eyes that had received PC in the past still had active NV, wide NPA, and IRMAs for which PC was not performed. Patients with mild diabetic macular edema (nontreated) were also included. However, all patients who required anti-VEGF therapy before PRP were excluded because anti-VEGF therapy would in this study greatly affect the morphological

Investigative Ophthalmology & Visual Science

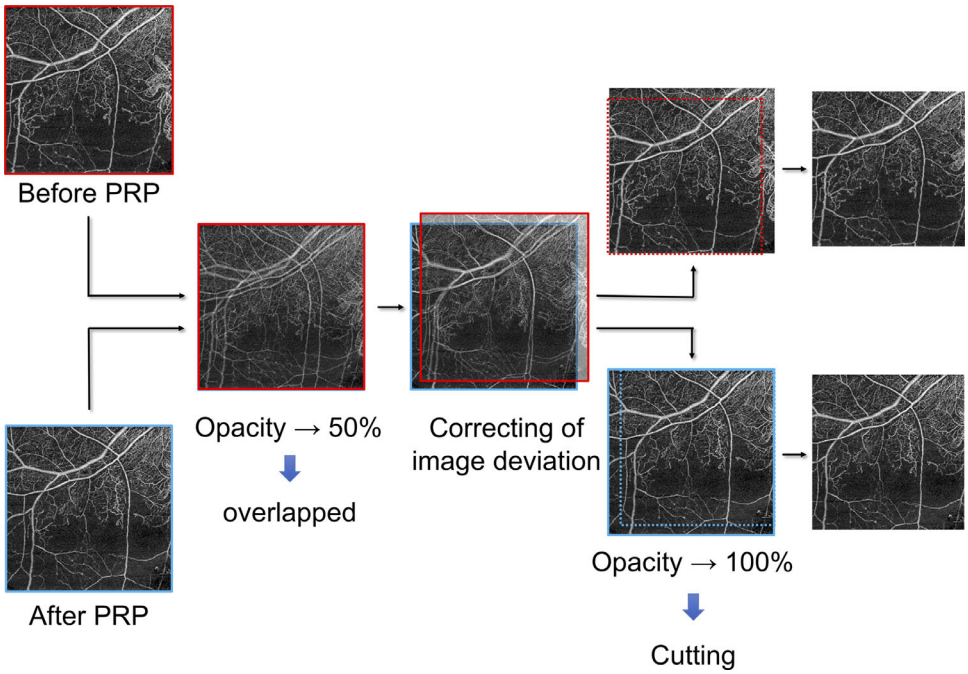

Figure 2. Flowchart of image trimming steps for image analysis using Adobe Photoshop. The OCTA images were obtained before (*red square*) and after (*blue square*) PRP. First, one of the obtained images is overlapped with 50% opacity. Second, the image deviation is corrected with reference to running of the blood vessels. Third, returning the opacity to 100% and creating an image that cuts out only the overlapped area (*red and blue dotted square*).

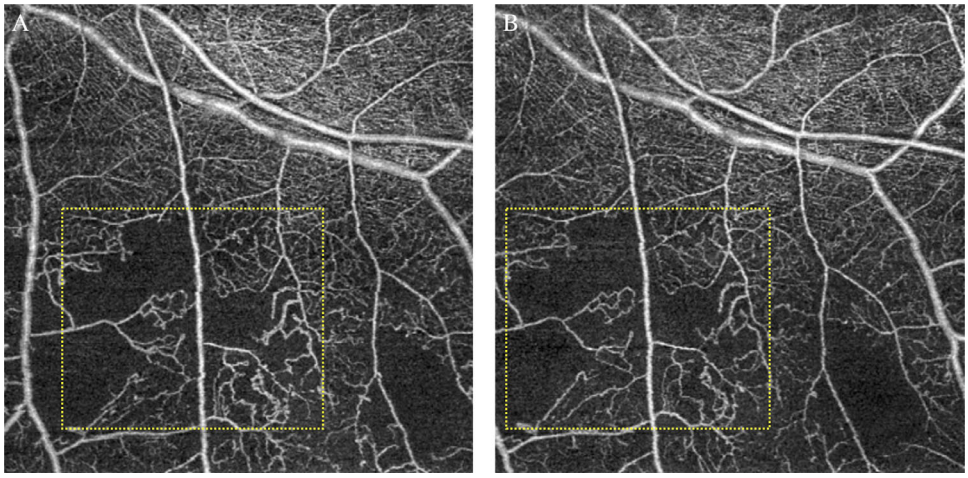

Figure 3. The morphology of IRMAs in the unchanged type. (**A**) OCTA image clearly shows the morphology of IRMAs existing in contact with the NPA before PRP (*yellow dotted square*). (**B**) OCTA image after PRP in the same place. There is no change in the morphology of IRMAs (*yellow dotted square*).

analysis of IRMA. The exclusion criteria were patients with any other retinal disorders, including a history of vitreous surgery and the presence of media opacities, such as severe vitreous hemorrhage and cataract, and previous treatment with an intravitreous injection of anti-VEGF drugs.

Disease severity was evaluated on the basis of the International Clinical Diabetic Retinopathy and Diabetic Macular Edema Disease Severity Scales using slit-lamp biomicroscopy, CFP (a TRC-50DX [Topcon, Tokyo, Japan] or Optos 200Tx [Optos PLC, Dunfermline, Scotland] retinal camera), and FA (Spectralis HRA + OCT [Heidelberg Engineering, Heidelberg, Germany] or Optos 200Tx).[6] All patients underwent comprehensive ophthalmologic examinations, including measurement of best-corrected visual acuity, intraocular pressure, slit-lamp biomicroscopy, CFP, FA, optical coherence tomography (OCT) (Topcon DRI OCT Triton Swept-source OCT [Topcon] and the RTVue-XR Avanti [Optovue, Inc, Fremont, California, USA]), and OCTA. FA and OCTA were performed before PRP and at 1 month after PRP completion. PRP was applied in four sessions at an interval of 14 days between treatment.

Investigative Ophthalmology & Visual Science

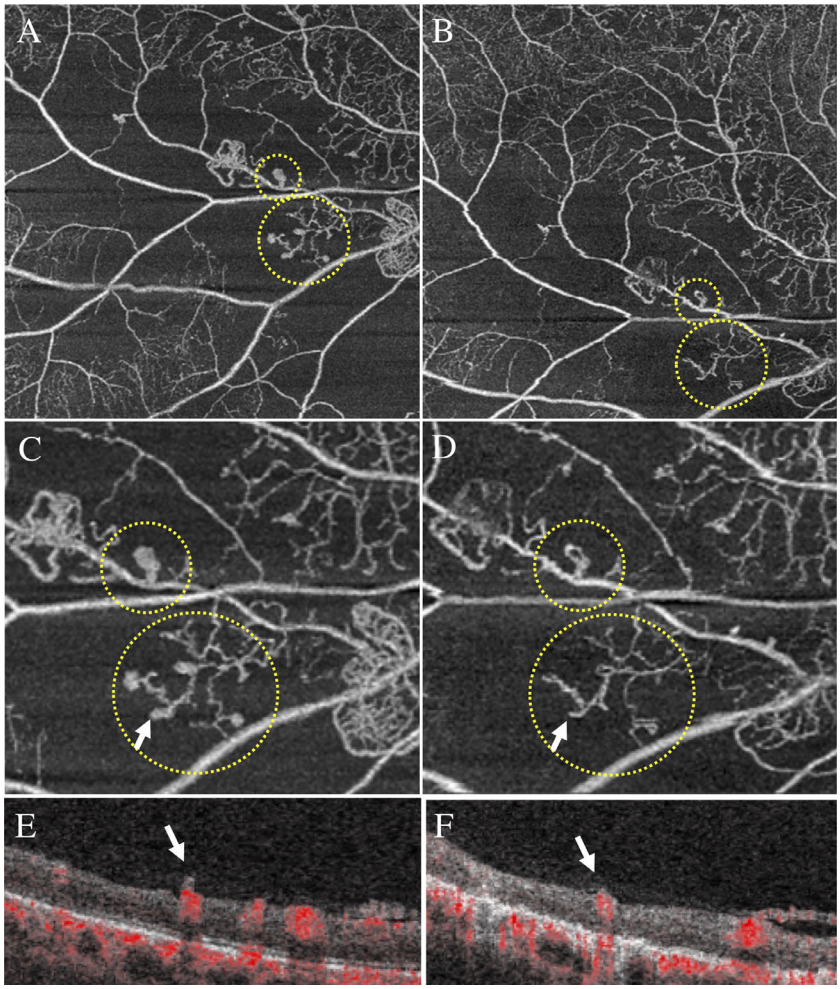

Figure 4. The morphological changes of IRMAs before and after PRP in the tuft-regression type. (**A**) The findings of IRMAs in the 6 × 6-mm area observed by OCTA before PRP. (**B**) The findings of IRMAs observed by OCTA after PRP. (**C**) Magnified view of the IRMAs in the OCTA image before PRP. Some IRMAs had buds of massive new blood vessel (tufts) at the tip of the IRMA in the area adjacent to the NPA (*yellow dotted circle* and *white arrow*). (**D**) Magnified views of the IRMAs in the OCTA image after PRP. There is no change in the branches of IRMA, however, the tufts regressed and changed to a ring shape (*yellow dotted circle* and *white arrow*). (**E,F**) Horizontal B-scan images show layer segmentation of the tufts with *white arrows* in the corresponding en face OCT angiograms shown in (**C**) and (**D**), respectively. The tuft originating from IRMA in the full retina tended to exceed the ILM before PRP (*white arrow* in **E**) and regressed after PRP (*white arrow* in **F**).

Therefore the time for evaluation of the IRMA after PRP was 3 months after starting PRP, which was performed with the following parameters: 200-ms pulse duration, 200-μm spot size, and 120- to 160-mW power. A conventional laser was applied to the middle peripheral area outside the arcade, including the IRMAs evaluated in this study, and a pattern-scanning laser was added to the peripheral area. The average number of shots was 3627 burns (range, 1700–4900). The following systemic clinical data were also recorded for all participants at the time of ophthalmic examination: body mass index, blood pressure, history of hypertension, type of diabetes mellitus, hemoglobin A1c level, duration of diabetes, and history of insulin treatment.

Optical Coherence Tomography Angiography

The instrument used for the OCTA images was based on the Zeiss Cirrus 5000 with AngioPlex OCTA software (Carl Zeiss Meditec, Inc., Dublin, CA, USA), with an A-scan depth of 2 mm, an axial resolution of 5 μm, and a transverse resolution of 15 μm. The software generated flow images using the OCT micro-angiography-complex algorithm, which incorporates differences in both the phase and intensity information, and FastTrac (15 fps) retinal tracking technology to reduce motion artifacts.[17] The scanning area for OCTA was selected on the basis of the identification of IRMAs in CFP and FA images (Fig. 1). IRMAs were imaged by moving the software scanning area and changing the built-in fixation point before PRP using en face angiograms (6 × 6 mm) around the optic disk and vascular arcades. At 3 months after starting PRP, IRMAs at the same location were re-evaluated with FA and OCTA. For the purposes of this study, only OCTA images with a signal strength >6/10 were used.

Evaluation of IRMAs

Morphology of IRMAs was evaluated in 6 × 6-mm en face OCTA images, and we used whole-retina segmentation for analysis. To observe the IRMA and new vessels on each en face OCT angiogram, segmentation of the inner border on

Investigative Ophthalmology & Visual Science

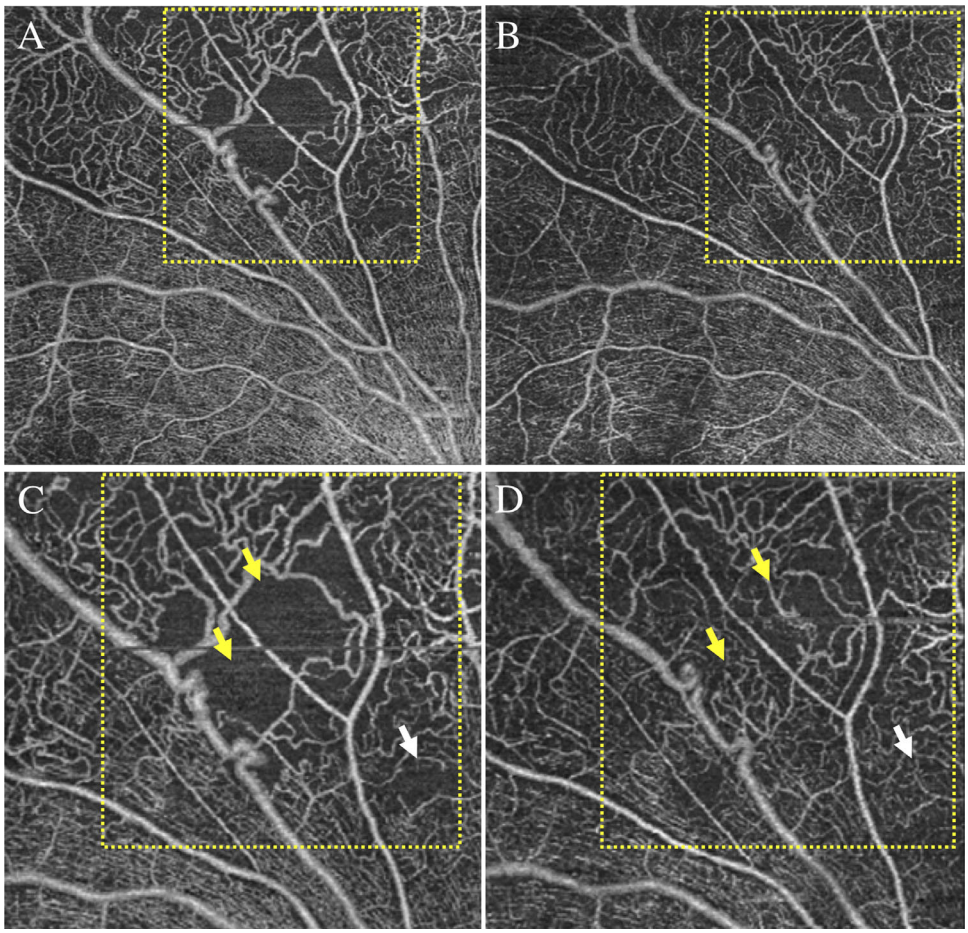

Figure 5. The morphological changes in IRMAs before and after PRP in the reperfusion type. (**A**) The findings of IRMAs in the 6 × 6-mm area observed by OCTA before PRP. (**B**) The findings of IRMAs observed by OCTA after PRP. (**C**) Magnified view showing the NPA in which flow signal is not confirmed (*white and yellow arrows*), and the remarkable extension and tortuous IRMAs before PRP (*yellow dotted square*). (**D**) Magnified view showing that a new flow signal is recognized in the NPA and tortuous blood vessels varying in caliber have improved (*yellow dotted square*). The reperfusion vessels show two vascular patterns; abnormal (dilated, tortuous, and twisted: *yellow arrow*) and normal (*white arrow*) blood vessels.

the B-scan was manually moved at the vitreous cavity, and the outer border was set at the inner plexiform layer. All IRMAs in the scanning area were evaluated. We confirmed the presence of IRMAs using the B-scan OCT images with overlaid flow signal. We distinguished between IRMAs and NV according to whether the ILM was exceeded, such that NV was defined by the disruption of the ILM and growth into the posterior hyaloid. IRMAs were defined as being fully retinal and not exceeding the ILM. Evaluations were performed on images taken before PRP and 3 months after start of PRP. Although this period was not a long-term observation, it was sufficiently long to evaluate the morphological changes in the IRMAs because the neovascularization at disk and NVE in our previous study certainly regressed during this term.[16] To evaluate the morphological changes in IRMAs, the corresponding before and after PRP images were input into Photoshop (Adobe, San Jose, CA, USA) and the overlapping ranges cut out (Fig. 2).

In the current study, the morphological changes in the IRMAs were divided into five subtypes: (1) unchanged type; (2) tuft-regression type; (3) reperfusion type; (4) mixed type; and (5) worsening type. The unchanged type was defined as no change in the morphology of IRMA before and after PRP (Fig. 3). The tuft-regression type demonstrated that the tufts (buds of massive new blood vessel) were present in pre-PRP images but regressed after PRP (Fig. 4). We defined a tuft as being part of an IRMA, mainly present at the tip of an IRMA in contact with an NPA, and as having a diameter more than twice that of capillaries, a closed end, and a bulging shape. The reperfusion type had no-signal area in pre-PRP images but showed that capillary perfusion within the NPA was partially recovered after PRP (Fig. 5). We considered not only the recovery of normal capillaries but also abnormal (dilated, tortuous, and twisted) blood vessels as the reperfusion type. In the no-signal area, it was confirmed that there was no perfusion even in FA. The mixed type was defined as having characteristics of both the tuft-regression and reperfusion types in the same OCTA image (Fig. 6). The worsening type demonstrated new tufts in NPAs after PRP (Fig. 7). The types of the IRMAs on the OCTA images were graded by two independent retinal specialists (AI and AS). When discrepancies occurred between the results, they were openly discussed, and a conclusive decision reached. Any gradings that did not achieve agreement by discussion were excluded from the analysis. In this study, we observed IRMAs in a limited area of 6 × 6 mm, not the entire retina. Moreover, some

Investigative Ophthalmology & Visual Science

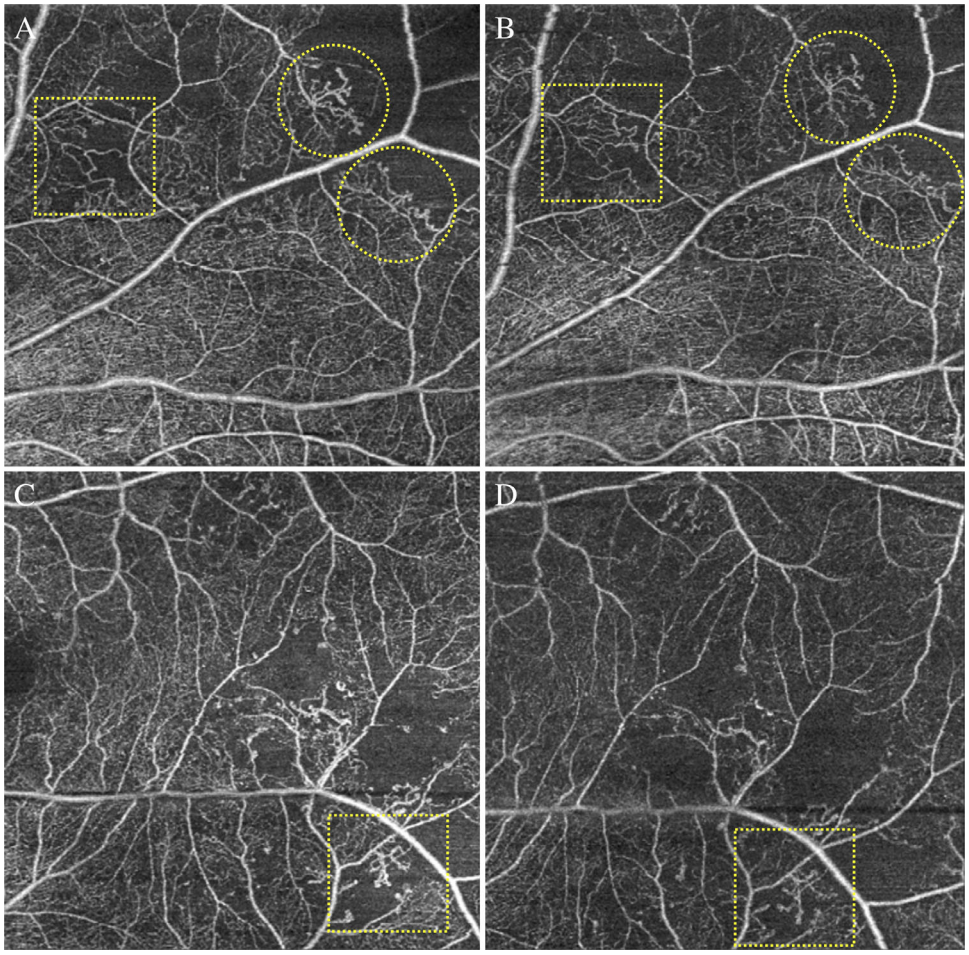

Figure 6. The morphological changes in IRMAs before and after PRP in the mixed type. (**A**) The findings of IRMAs in the 6 × 6-mm area observed by OCTA before PRP. There are NPAs and some IRMAs with tufts (*dotted circle*). (**B**) OCTA image showing that reperfusion in NPA (*yellow dotted square*) and regression of tufts (*yellow dotted circle*) exist in different IRMAs within the same 6 × 6-mm OCTA image. (**C**) The 6 × 6-mm OCTA image of another patient before PRP. There are NPAs and some IRMAs that have tufts at the tip in contact with the NPA (*dotted square*). The reperfused vessels are connected to surrounding vessels, and the vessel diameter is normal. (**D**) In the same IRMA, the tufts regressed, and the tip of the IRMA extended, so another two properties of reperfusion and tuft-regression type are mixed. Reperfused vessels are dilated, tortuous, and have a closed end.

IRMAs were isolated but fused each other, so we evaluated at least one unit of IRMAs in the 6 × 6-mm OCTA images.

Statistical Analyses

The distribution of numeric variables was assessed by inspecting histograms and using the D'agostino–Pearson normality test. All data were expressed as the mean ± SD. The Fisher's exact test was used for categorical variables. To assess reliability for grading of IRMA between the graders (AS and AI), Cohen's Kappa was calculated. To evaluate whether tufts could be predictors of progression to PDR, the data were divided into two groups of with and without tufts before treatment, and the proportions in SNPDR and PDR were analyzed. Paired *t*-tests were used to compare the mean signal strength in the OCTA images between the before and after PRP images. SPSS v25 (IBM Corporation, Armonk, NY, USA) and Prism 7 (GraphPad Software, Inc., La Jolla, CA, USA) were used for statistical analysis, and a P value <0.05 was considered to be indicative of statistical significance.

Results

Baseline Characteristics

The study included 46 eyes of 29 patients (19 men, 10 women). The patients ranged in age from 29 to 78 years, with a mean age of 60.7 years. Twenty-six eyes were diagnosed as having SNPDR, and 20 eyes were diagnosed as having PDR. Table 1 presents the demographic and clinical characteristics of the study patients.

Difference Between Visualization in FA and OCTA

First, FA confirmed the presence of IRMAs, NPA, and NV, and activity of DR in all eyes. Later, the same lesions were confirmed by using OCTA guided by FA images. Pre-PRP FA images allowed visualization of the degree of DR severity and localization of NPA, active NV, and IRMAs; however, they could not clearly visualize details of NV and IRMAs because of fluorescein leakage from NV. Post-PRP FA images could not clearly demarcate the NPA because of PC spots.

Investigative Ophthalmology & Visual Science

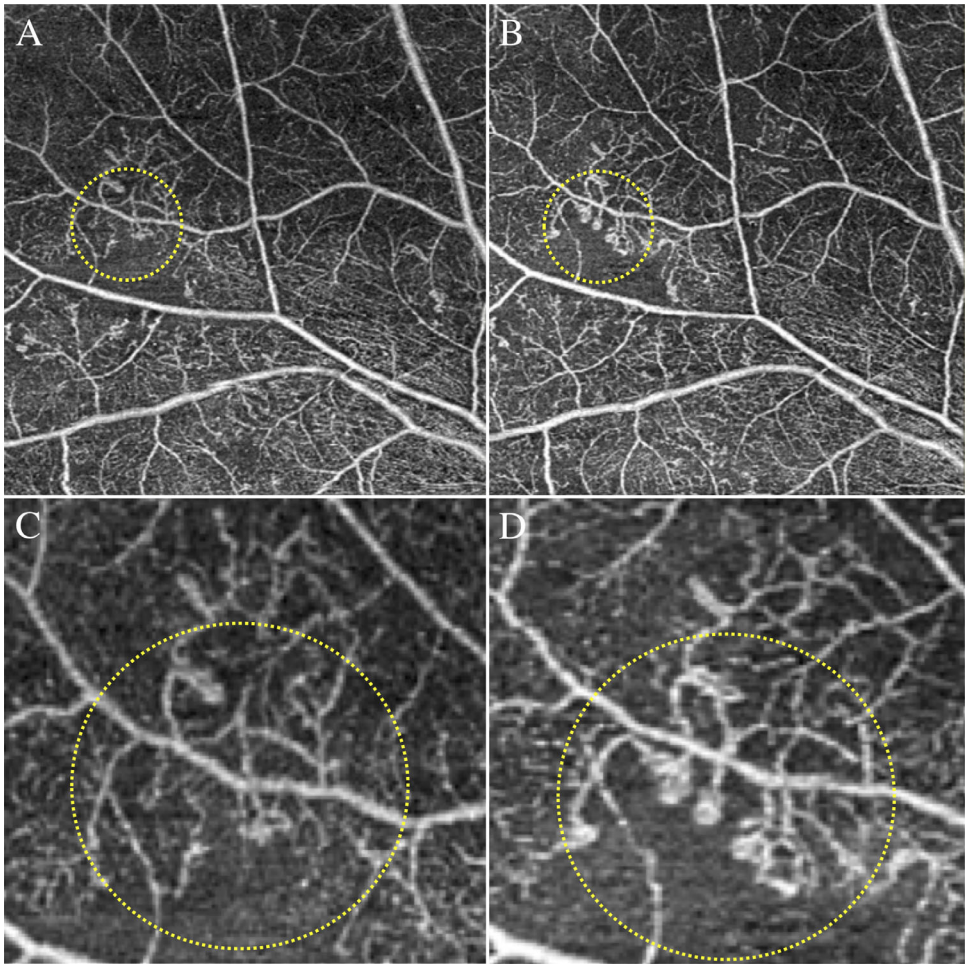

Figure 7. The morphological changes in IRMAs before and after PRP in the worsening type. (**A**) The findings of IRMAs in the 6 × 6-mm area observed by OCTA before PRP. (**B**) IRMAs observed by OCTA after PRP. (**C**) Magnified view showing IRMAs in the NPA (*yellow dotted circle*). (**D**) Magnified view showing the formation of a new tuft at the tip of the IRMA in contact with the NPA.

OCTA images, however, allowed visualization of all necessary image components (Fig. 8).

Morphological Changes in IRMAs Before and After PRP

Using the en face whole-layer OCTA images, we performed the IRMA grading. The mean signal strength (maximum value of 10) in OCTA images was not significantly different before (8.4 ± 1.0; range, 6–10) and after (8.2 ± 1.1; range, 6–10) PRP. Table 2 shows the proposed subclassification of IRMAs focusing on the presence of tufts, recovery of capillary perfusion, and ratio of subtypes in each stage of DR. The IRMA grading between the two examiners showed a high rate of agreement (Cohen's kappa = 0.817). In SNPDR-diagnosed eyes, the unchanged type was observed in 15 eyes, accounting for the majority, whereas in PDR-diagnosed eyes, only two eyes were observed. Before treatments, tufts were more frequently observed in eyes with PDR (15/20 eyes, 75%) than in eyes with SNPDR (8/26 eyes, 31%) ($P = 0.003$; Table 2). In tuft-regression type patients with PDR, the tufts originating from IRMA in the full retina tended to exceed ILM in two eyes before PRP, and those tufts regressed after PRP (Figs. 4E, 4F). The worsening type was observed in 3 eyes (1/26 SNPDR eyes and 2/20 PDR eyes, the average number of shots was 4233 burns [range, 3000–5800]) for 46 eyes and seemed to be rare events. The reperfusion type was observed in three eyes (2/26 SNPDR eyes and 1/20 PDR eyes). However, the phenomenon of reperfusion was observed in 11 eyes (7/26 SNPDR eyes and 4/20 PDR eyes), including the mixed type.

Discussion

In this study, we compared the morphological changes in IRMAs in DR before and after PRP by using OCTA images to better delineate the detailed structure of the IRMAs. To our knowledge, this is the first study to investigate the pathophysiology of IRMAs in detail. FA is an important imaging method and is particularly useful for evaluating the degree of macular edema and as an adjunct for classifying the severity of DR.[18–20] Although the leakage of fluorescein can be an indicator of NV activity, it can be difficult to distinguish IRMA from small or faintly leaking NVs. Furthermore, fluorescein leakage and PC scars interfere with the observation of NV, IRMA, and NPA. However, OCTA is a noninvasive technique and can provide clearer structural details of NVs and IRMAs

Investigative Ophthalmology & Visual Science

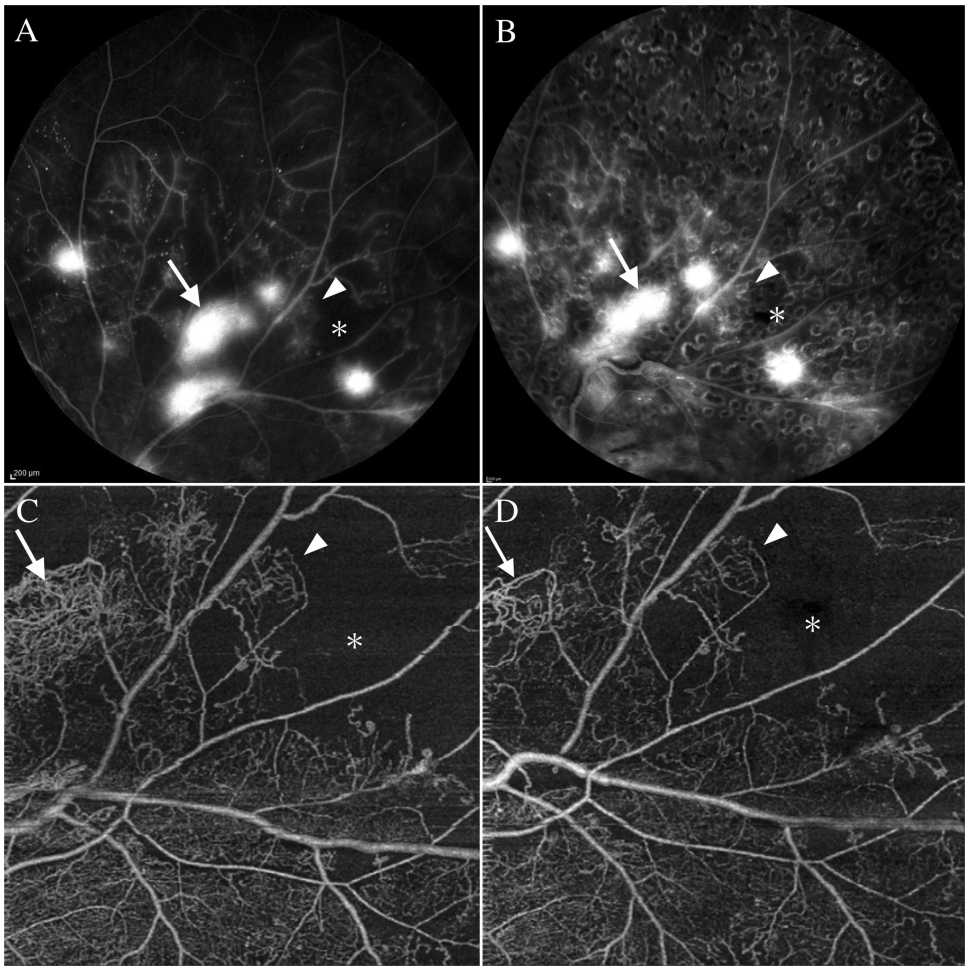

Figure 8. Comparison of findings of NV, IRMAs, and the NPA between FA and OCTA before and after PRP. (**A**) FA images of NV (*arrow*), IRMA (*arrowhead*), and NPA (*asterisk*) before PRP. There is a remarkable fluorescence leakage from the NV, and mild fluorescence leakage from IRMAs, so the details of these morphologies cannot be seen clearly. (**B**) In the FA image after PRP, there is no obvious change in the degree of leakage from the NV. The localization of the IRMA and the extent of the NPA are not clear by laser scar. (**C**) OCTA findings in the 6 × 6-mm area at the same location as the FA before PRP. The *white arrow* indicates the NV with irregular proliferation of fine vessels. Without being affected by fluorescence leakage, the detailed morphology of IRMA and the extent of the NPA can be clearly confirmed. (**D**) OCTA findings of the 6 × 6-mm area after PRP showing a pruned and contracted NV (*arrow*). In contrast, there is no obvious change in the IRMA and NPA.

without obscuration by PC scars and FA leakage.[14] Additionally, wide-field OCTA has high sensitivity and specificity for the detection of the NPA and NVs.[14,21–23] In our study, OCTA clearly visualized NV, IRMAs, and the NPA without being affected by PC scars. Moreover, it was possible to distinguish NVs from IRMAs by confirming B-scans.[13]

All NVs observed on OCTA images exhibited signs of pruning, and the heavily developed, fine abnormal vessels within NVs were regressed, as reported previously (Fig. 8).[16] This finding has suggested that NV activity was decreased because of reduction by PRP of the intraocular VEGF concentration.[24] However, some of the IRMAs in the SNPDR eyes, which we defined herein as the unchanged type, showed no morphological changes before and after PRP. This finding would suggest that IRMAs might represent vascular remodeling of existing capillaries without NV.

In the reperfusion type, blood flow was restored in areas where a flow signal was not detected by OCTA, and where IRMAs appeared to have improved (Fig. 5). Several mechanisms underlying vascular occlusion in DR have been demonstrated. VEGF has a particularly important role in vascular occlusion in DR by inducing hypertrophy of vascular endothelial cells[25] and leukostasis caused by adhesion molecules, such as ICAM-1.[26–31] PC in retinal ischemia destroys photoreceptors that require a large amount of oxygen, which yields areas of increased oxygenation that reduces the ischemic retinal area, and lowers VEGF production by the ischemic retinal tissue. Additionally, OCTA cannot detect the blood flow signal at low perfusion levels. Thus the reduction of intraocular VEGF concentration following PC should hypothetically improve leukostasis and vascular endothelial cell hypertrophy and ultimately correct the reversible vascular occlusion. However, Powner et al.[35] in their study suggested that an en face OCT signal originates from the vessel wall with progressive loss of vascular cells (endothelial cells and pericytes) over time. The remaining acellular basement membrane tubes (ghost vessels) were preserved for many years. In the current study, the ghost vessels may have been present in accordance with the regions that were reperfused after PRP. However,

Investigative Ophthalmology & Visual Science

Table 1. Patients Characteristics and Ocular Parameters of the Enrolled Eyes

Variables	Mean ± SD (Range)
All patients, *n*	29
Age, y	60.7 ± 12.3 (29–78)
Sex, *n* (%)	
Male	19 (65.5%)
Female	10 (34.5%)
Body mass index	25.5 ± 5.0 (17.2–37.3)
Blood pressure, mm Hg	
Systolic	140.7 ± 17.3 (111–175)
Diastolic	77.3 ± 11.0 (55–97)
Mean	98.4 ± 11.2 (73.7–115.3)
History of hypertension, *n* (%)	14 (48.3%)
Type of diabetes mellitus, *n* (%)	
Type 1	1 (3.4%)
Type 2	28 (96.6%)
HbA1c, %	7.9 ± 1.6 (5.2–11.4)
Duration of diabetes, y	11.9 ± 10.6 (0.2–50)
History of insulin treatment, *n* (%)	11 (37.9%)
All eyes, *n*	46
BCVA, logMAR	0.10 ± 0.3 (−0.08 to 1)
IOP, mm Hg	15.7 ± 4.0 (10–25)
Central macular thickness, μm	308.5 ± 83.8 (176–597)
Severity of DR, *n* (%)	
SNPDR	26 (56.5%)
PDR	20 (43.5%)

BCVA, best-corrected visual acuity; IOP, intraocular pressure.

capillary-level ghost vessels may be hardly observed in en face OCT images obtained by OCTA. Therefore further study is needed to investigate the relationship between the reperfusion type of IRMA and ghost vessels.

Alternatively, reperfusion could be related to IRNVs.[11] Takahashi et al.[12] in their study reported that reperfusion of occluded capillary beds was observed in DR without treatment, noting two distinct patterns of reperfusion distinguished by the presence of abnormal (IRNVs) or normal (recanalization) blood vessels. They indicated that the vascular pattern of the recanalized capillary beds was similar to that of adjacent intact capillary beds. In contrast, IRNVs formed a dilated, coarse, and zigzag-running new capillary networks by slowly growing of buds into the NPA. The IRNVs differed from the vascular pattern of the adjacent capillary beds and showed that, in some cases, the remodeling of capillaries, venules, and arterioles occurred for several years in the area of reperfused capillary beds. In our study, Figure 5 shows the new capillary beds in the NPA after PRP. The reperfusion vessels showed two vascular patterns; abnormal (dilated, tortuous, and twisted: yellow arrow) and normal (white arrow) blood vessels. Also, Figure 6 shows that reperfused vessels are dilated and tortuous and have a closed end, and NPA are reperfused incompletely. These characteristics are consistent with the two distinct patterns of reperfusion observed in the study by Takahashi et al.[12] When observed over longer periods, these may be a remodeling process as in the previous report.

In the tuft regression type, some of the IRMAs had tufts at the tip of the IRMA in the area adjacent to the NPA, similar to those observed in rodent models of the oxygen-induced retinopathy.[32] IRMAs with tufts were found in 75% of the PDR eyes before treatment, which was significantly more than those found in SNPDR (Table 2). Additionally, all tufts regressed after PRP, as did NV (Fig. 4). Some of the regressed tufts might be indistinguishable from microaneurysms; however, the tufts not only regressed but also exhibited a distinct ring shape after PRP, which was different from that of a microaneurysm. This ring shape was believed to reflect the inability of OCTA to detect the signal of blood flow due to congested circulation in the tuft. Additionally, the tuft has several different morphological characteristics from those of a microaneurysm. Tufts existed at the tip of the IRMA in contact with the NPA and has a diameter more than twice that of capillaries, a closed end, and has a bulging shape. Lee et al.[13] in their study reported that IRMAs followed longitudinally progressed to NVs, and the transition from IRMA to NV commenced with an initial outpouching of the ILM without disruption of this layer. It has been suggested that once there is disruption of the ILM, the early neovascular complex grows into the potential space between the ILM and posterior hyaloid.[13] The underlying mechanism is thus thought to be attributable to leakage from the vessels that then create a focal detachment of the vitreous fluid into which new vessels can grow.[33,34] Lee et al.[13] in their study reported progression of IRMAs in the vertical direction toward the vitreous side based on the spectral-domain-OCT images, but progression in the horizontal direction toward the NPA was not clear. We revealed that two of the tufts progressed in the direction of the NPA and tended to exceed the ILM in the area that is in contact with the posterior hyaloid before PRP. These tufts were regressed after PRP (Figs. 4E, 4F). Additionally, in rare cases new tufts formed after PRP (Fig. 7). The worsening type was observed in one SNPDR and two PDR eyes. These eyes received insufficient PRP and were active as shown on FA image even after PRP. Pan et al.[10] in their study reported the presence of NV as originating from IRMA. However, Takahashi et al.[12] in their study reported that the NV was initiated as budding from venules, and the projected buds slowly grew into the NPA. They also reported that some IRNVs developed into preretinal NV.[12] Therefore some of these buds they described may have become tufts. These results suggest that some types of IRMAs and IRNVs can develop into NVs. Formation of tufts may be an indicator of progression from SNPDR to PDR. However, a prospective study is necessary to prove this.

We here defined a type with both tuft-regression and reperfusion characteristics in the same OCTA image as the "mixed type." In the mixed type, two types were found in different IRMAs within the same 6 × 6-mm OCTA image (Figs. 6A, 6B). However, we found that there are some cases in which two properties coexist in the same IRMA (Figs. 6C, 6D). Even though these are defined as the same mixed type, they are considered to be different. Especially in the type with two properties in the same IRMA, the reperfused vessels had abnormally running and morphology, which suggested the possibility of IRNV. In the current study, there were no cases in which the worsening type and other types existed in the same retina.

There were several limitations in our study. First, selection bias cannot be completely eliminated. Because the part of the retina is selected and evaluated manually, the whole retina was not evaluated. However, in our study, we confirmed that the IRMA type in the selected 6 × 6-mm image had the same tendency as the IRMA type existing in other regions of the same retina, and therefore the effect of selection bias seemed to have been minimal. To further minimize the selection bias as much as possible, it is necessary to use the wide-field OCTA in a future study. Next, there is a limit to the OCTA technique for

Table 2. Proposed Subclassification of IRMAs and the Ratio of Subtypes in Each Stage of DR

Type of IRMA	Characteristic	SNPDR	PDR	*P* Value
Unchanged	No change after PRP	15 (57)	2 (10)	
Tuft regression	Tufts are not visible or diminished after PRP	3 (12)	12 (60)	0.003*
Reperfusion	Capillary perfusion within NPA is partially recovered after PRP	2 (8)	1 (5)	
Mixed	Tuft-regression + reperfusion	5 (19)	3 (15)	
Worsening	New tufts appear after PRP	1 (4)	2 (10)	

Data show the total number and percentage of total number in each stage.
* *P* value is for the comparison between the ratio of IRMA with (tuft-regression and mixed) and without (others) tuft before treatment in each stage of DR.

detection of subtle changes in IRMAs. OCTA cannot detect signals below the detection sensitivity at low perfusion rates. Therefore we confirmed that there was no perfusion, even in FA images in the same area as OCTA images. Additionally, evaluation of IRMA changes may be affected by signal strength. If the signal strength is low, details of IRMA cannot be observed. Even if there is perfusion, it cannot be detected, so it may appear as if reperfusion has occurred by improving the signal strength. Therefore we used only OCTA images with a signal strength >6/10 and confirmed that the mean signal strength in OCTA images was not significantly different before and after PRP. In our study, we did not observe long-term changes in IRMAs. Therefore regarding the stage of IRMA, further examination is necessary to determine if it is an independent process or a transition from the remodeling process to the angiogenic process. A future prospective study including more long-term observation over several years is essential to investigate the changes in IRMAs in detail. Another limitation of our analysis was that we did not directly measure intraocular VEGF concentration. We estimated the degree of the FA leak and NV reduction. Additionally, the all-scanned areas that included IRMAs were treated with a conventional laser. A pattern-scanning laser was also used in the peripheral retina, and there were variations in the number of laser shots. Therefore it was difficult to evaluate the effect of the number of laser shots on the IRMAs. As such, a more detailed investigation is needed on the relationship between changes in IRMAs and VEGF concentration.

Conclusions

This study demonstrated that OCTA can clearly visualize morphological changes in IRMAs before and after PRP, which enabled classification of IRMA into more detailed types. Additionally, this study suggested that IRMA might have developed via both remodeling and NV. Observing morphological changes in IRMAs may enable earlier detection of severe DR signs and potentially lead to earlier treatment.

Acknowledgments

Supported by Novartis Pharma Research Grants 2017, Grant-in-Aid for Young Scientists (AS, 19K18866), and Grant-in-Aid for Scientific Research (AI, 19K09925).

Disclosure: **A. Shimouchi,** None; **A. Ishibazawa,** None; **S. Ishiko,** None; **T. Omae,** None; **T. Ro-Mase,** None; **Y. Yanagi,** None; **A. Yoshida,** None

References

1. Grading diabetic retinopathy from stereoscopic color fundus photographs–an extension of the modified Airlie House classification. ETDRS report number 10. Early Treatment Diabetic Retinopathy Study Research Group. *Ophthalmology.* 1991;98(5 suppl):786–806.
2. van Dijk HW, Verbraak FD, Kok PH, et al. Decreased retinal ganglion cell layer thickness in patients with type 1 diabetes. *Invest Ophthalmol Vis Sci.* 2010;51:3660–3665.
3. Diabetic retinopathy study. Report number 6. Design, methods, and baseline results. Report number 7. A modification of the Airlie House classification of diabetic retinopathy. Prepared by the Diabetic Retinopathy. *Invest Ophthalmol Vis Sci.* 1981;21:1–226.
4. Early Treatment Diabetic Retinopathy Study design and baseline patient characteristics. ETDRS report number 7. *Ophthalmology.* 1991;98(5 suppl):741–756.
5. Fundus photographic risk factors for progression of diabetic retinopathy. ETDRS report number 12. Early Treatment Diabetic Retinopathy Study Research Group. *Ophthalmology.* 1991;98(5 suppl):823–833.
6. Wilkinson CP, Ferris FL, 3rd, Klein RE, et al. Proposed international clinical diabetic retinopathy and diabetic macular edema disease severity scales. *Ophthalmology.* 2003;110:1677–1682.
7. Ashton N. Arteriolar involvement in diabetic retinopathy. *Br J Ophthalmol.* 1953;37:282–292.
8. Davis MD, Blodi BA. Proliferative diabetic retinopathy. In: Ryan SJ , ed. *Retina.* 4th ed. Philadelphia: Elsevier/Mosby; 2006:1285–1322.
9. Lee C. Diabetic retinopathy. In: Spaide RF , ed. *Diseases of the Retina and Vitreous.* Philadelphia, PA: WB Saunders Company; 1999:129–143.
10. Pan J, Chen D, Yang X, et al. Characteristics of neovascularization in early stages of proliferative diabetic retinopathy by optical coherence tomography angiography. *Am J Ophthalmol.* 2018;192:146–156.
11. Muraoka K, Shimizu K. Intraretinal neovascularization in diabetic retinopathy. *Ophthalmology.* 1984;91:1440–1446.
12. Takahashi K, Kishi S, Muraoka K, Shimizu K. Reperfusion of occluded capillary beds in diabetic retinopathy. *Am J Ophthalmol.* 1998;126:791–797.
13. Lee CS, Lee AY, Sim DA, et al. Reevaluating the definition of intraretinal microvascular abnormalities and neovascularization elsewhere in diabetic retinopathy using optical coherence tomography and fluorescein angiography. *Am J Ophthalmol.* 2015;159:101–110.e101.
14. Ishibazawa A, Nagaoka T, Takahashi A, et al. Optical coherence tomography angiography in diabetic retinopathy: a prospective pilot study. *Am J Ophthalmol.* 2015;160:35–44.e31.
15. Schaal KB, Munk MR, Wyssmueller I, Berger LE, Zinkernagel MS, Wolf S. Vascular abnormalities in diabetic retinopathy

assessed with swept-source optical coherence tomography angiography widefield imaging. *Retina*. 2019;39:79–87.

16. Ishibazawa A, Nagaoka T, Yokota H, et al. Characteristics of retinal neovascularization in proliferative diabetic retinopathy imaged by optical coherence tomography angiography. *Invest Ophthalmol Vis Sci*. 2016;57:6247–6255.
17. Rosenfeld PJ, Durbin MK, Roisman L, et al. ZEISS angioplex spectral domain optical coherence tomography angiography: technical aspects. *Dev Ophthalmol*. 2016;56:18–29.
18. Focal photocoagulation treatment of diabetic macular edema. Relationship of treatment effect to fluorescein angiographic and other retinal characteristics at baseline: ETDRS report no. 19. Early Treatment Diabetic Retinopathy Study Research Group. *Arch Ophthalmol*. 1995;113:1144–1155.
19. Treatment techniques and clinical guidelines for photocoagulation of diabetic macular edema. Early treatment diabetic retinopathy study report number 2. Early Treatment Diabetic Retinopathy Study Research Group. *Ophthalmology*. 1987;94:761–774.
20. Classification of diabetic retinopathy from fluorescein angiograms. ETDRS report number 11. Early Treatment Diabetic Retinopathy Study Research Group. *Ophthalmology*. 1991;98:807–822.
21. Salz DA, de Carlo TE, Adhi M, et al. Select features of diabetic retinopathy on swept-source optical coherence tomographic angiography compared with fluorescein angiography and normal eyes. *JAMA Ophthalmol*. 2016;134:644–650.
22. Matsunaga DR, Yi JJ, De Koo LO, Ameri H, Puliafito CA, Kashani AH. Optical coherence tomography angiography of diabetic retinopathy in human subjects. *Ophthalmic Surg Lasers Imaging Retina*. 2015;46:796–805.
23. Sawada O, Ichiyama Y, Obata S, et al. Comparison between wide-angle OCT angiography and ultra-wide field fluorescein angiography for detecting non-perfusion areas and retinal neovascularization in eyes with diabetic retinopathy. *Graefes Arch Clin Exp Ophthalmol*. 2018;256:1275–1280.
24. Aiello LP, Avery RL, Arrigg PG, et al. Vascular endothelial growth factor in ocular fluid of patients with diabetic retinopathy and other retinal disorders. *N Engl J Med*. 1994;331:1480–1487.
25. Hofman P, van Blijswijk BC, Gaillard PJ, Vrensen GF, Schlingemann RO. Endothelial cell hypertrophy induced by vascular endothelial growth factor in the retina: new insights into the pathogenesis of capillary nonperfusion. *Arch Ophthalmol*. 2001;119:861–866.
26. Joussen AM, Poulaki V, Qin W, et al. Retinal vascular endothelial growth factor induces intercellular adhesion molecule-1 and endothelial nitric oxide synthase expression and initiates early diabetic retinal leukocyte adhesion in vivo. *Am J Pathol*. 2002;160:501–509.
27. Wierusz-Wysocka B, Wysocki H, Siekierka H, Wykretowicz A, Szczepanik A, Klimas R. Evidence of polymorphonuclear neutrophils (PMN) activation in patients with insulin-dependent diabetes mellitus. *J Leukoc Biol*. 1987;42:519–523.
28. Arnould T, Michiels C, Remacle J. Increased PMN adherence on endothelial cells after hypoxia: involvement of PAF, CD18/CD11b, and ICAM-1. *Am J Physiol*. 1993;264:C1102–C1110.
29. Lu M, Perez VL, Ma N, et al. VEGF increases retinal vascular ICAM-1 expression in vivo. *Invest Ophthalmol Vis Sci*. 1999;40:1808–1812.
30. Schroder S, Palinski W, Schmid-Schonbein GW. Activated monocytes and granulocytes, capillary nonperfusion, and neovascularization in diabetic retinopathy. *Am J Pathol*. 1991;139:81–100.
31. Joussen AM, Murata T, Tsujikawa A, Kirchhof B, Bursell SE, Adamis AP. Leukocyte-mediated endothelial cell injury and death in the diabetic retina. *Am J Pathol*. 2001;158:147–152.
32. Smith LE, Wesolowski E, McLellan A, et al. Oxygen-induced retinopathy in the mouse. *Invest Ophthalmol Vis Sci*. 1994;35:101–111.
33. Davis MD. Vitreous contraction in proliferative diabetic retinopathy. *Arch Ophthalmol*. 1965;74:741–751.
34. Constable IJ. Pathology of vitreous membranes and the effect of haemorrhage and new vessels on the vitreous. *Trans Ophthalmol Soc U K*. 1975;95:382–386.
35. Powner MB, Sim DA, Zhu M, et al. Evaluation of nonperfused retinal vessels in ischemic retinopathy. *Invest Ophthalmol Vis Sci*. 2016;57:5031–5037.

Investigative Ophthalmology & Visual Science